Reversible phase transition between amorphous phases in a bulk Zn-Sb alloy under high pressures

V. E. Antonov, O. I. Barkalov,* V. K. Fedotov, A. I. Harkunov, A. I. Kolyubakin, and E. G. Ponyatovsky
Institute of Solid State Physics RAS, 142432 Chernogolovka, Moscow District, Russia

M. Winzenick
Fachbereich Physik, Universität GH Paderborn, D-33095 Paderborn, Germany
(Received 22 February 1999)

A line of metastable equilibrium between two amorphous semiconductor phases was determined resistometrically in the *T-P* diagram of the $Zn_{41}Sb_{59}$ alloy in the temperature range from 17 to 75 °C. The amorphous nature of both phases was examined by x-ray diffraction at high pressures using a diamond-anvil cell and synchrotron radiation. The starting bulk amorphous sample was prepared by solid-state transformation of the quenched crystalline high-pressure δ-$Zn_{41}Sb_{59}$ phase during its heating at ambient pressure.

I. INTRODUCTION

Among the methods of solid-state amorphization, spontaneous amorphization of quenched high-pressure phases during their heating at ambient pressure is one of the most advantageous for producing bulk homogeneous samples.[1–3] Amorphous $Zn_{41}Sb_{59}$[4] and GaSb-Ge[5] produced by this method were studied previously at high pressures and it was shown that below the temperature of crystallization to the thermodynamic equilibrium state, the amorphous states can undergo reversible first-order phase transitions to other phases. The reversibility of the phase transitions evidences that these amorphous states are phases, i.e., they correspond to minima of the Gibbs potential. The amorphous phases are metastable and the minima therefore are not the deepest of all possible ones, but their presence gives an opportunity to describe transitions of these phases in the framework of equilibrium thermodynamics.

In the GaSb-Ge system, a reversible transition occurs between the amorphous semiconductor phase and the crystalline metallic high-pressure phase which was used before to produce this amorphous phase.[5] The behavior of the amorphous semiconductor $Zn_{41}Sb_{59}$ phase is quite different. With increase in pressure at room temperature, it undergoes two first-order phase transitions:[4] (i) a transition to another semiconductor phase near 2 GPa and (ii) a transition to a semimetallic phase around 5 GPa. The phase formed at pressures above 5 GPa was shown[6] to be a crystalline phase, called γ, with a simple hexagonal structure, different from the structure of the high-pressure δ phase used to prepare the initial amorphous phase. The 2-GPa transition was reversible and was accompanied by a 0.8% decrease in volume.[4] The structure of the semiconductor phase formed above 2 GPa was not studied immediately under pressure. Nevertheless, from the x-ray examination of the quenched $Zn_{41}Sb_{59}$ samples it was inferred that this phase is amorphous.

A reversible first-order phase transition between amorphous phases was earlier distinctly observed only in water, for two amorphous dielectric modifications of ice;[7] the corresponding metastable equilibrium phase diagram was calculated in Ref. 8. No transitions between amorphous semiconductor phases have been observed so far.

In the present work, the previous assumption[4] that the 2 GPa transition of the initially amorphous $Zn_{41}Sb_{59}$ is a transition between two amorphous phases, am_1 and am_2, was confirmed by *in situ* x-ray-diffraction experiments. The *T-P* region of thermal stability of the two amorphous phases with the transition lines for the forward $am_1 \rightarrow am_2$ and backward $am_2 \rightarrow am_1$ transition were determined by electrical resistance measurement. The $am_1 \rightleftarrows am_2$ metastable equilibrium was analyzed with the two-level model which was earlier applied successfully to construct the diagram of metastable equilibrium between the two modifications of amorphous ice and to describe the anomalous thermodynamic properties of these ices and liquid water.[8]

II. SAMPLE PREPARATION AND EXPERIMENTAL DETAILS

A 20-g ingot of a two-phase $Zn_{41}Sb_{59}$ alloy consisting of a mixture of semiconducting ZnSb and metallic antimony[9] was prepared from 99.99 wt % pure Zn and Sb by melting in an evacuated quartz tube and quenching into a cold water bath. The central part of the ingot was powdered in an agate mortar to obtain a more homogeneous ZnSb + Sb mixture and the powder was pressed into a pellet 8 mm in diameter and 5 mm thick. The pellet was put in a Teflon container, exposed to 7.5 GPa and 325 °C for 24 h in a Toroid-type high-pressure chamber and cooled to 100 K together with the chamber before the pressure was released. The x-ray examination at 100 K and ambient pressure (DRON-2.0 diffractometer, CuK_α radiation) showed in agreement with earlier results[10] that this procedure results in a complete transformation of the pellet to the high-pressure δ phase, which is stable at $P > 6.5$ GPa over a narrow concentration interval around the $Zn_{41}Sb_{59}$ composition. This pellet was then brought to the amorphous state by heating to room temperature and used to prepare the samples.

Energy dispersive x-ray diffraction (EDXD) on these samples under pressure was performed with synchrotron radiation and diamond-anvil cells (DAC) in HASYLAB at

DESY, Hamburg. A piece of amorphous $Zn_{41}Sb_{59}$ of nearly 150 μm diameter and around 20 μm thickness was loaded with white mineral oil and a few ruby grains into the central hole of the Inconel gasket in the DAC.[11,12] The spectra were recorded by a Ge detector at an angle of $2\Theta = 9.7174°$ over periods of 10 min in the course of the stepwise increase in pressure, which was measured by the ruby luminescence technique with a precision of ± 0.1 GPa with respect to the ruby scale.[13]

The electrical resistance was measured under pressure with samples in the form of bars 5–8 mm long and 1×1 mm^2 across cut from the pellet of amorphous $Zn_{41}Sb_{59}$ with an abrasive wire saw. Crystallization of the samples was studied in a Toroid-type quasihydrostatic high-pressure chamber using hexagonal BN as pressure transmitting medium; the resistance was measured by a dc four-probe method with copper electrodes pressed against the sample. The transition between the amorphous phases was investigated under hydrostatic conditions in a piston-cylinder hydrostatic cell filled with silicon oil; the resistance was measured by a two-probe technique using copper electrodes soldered to the sample with indium at 165 °C using ultrasonic soldering. Temperature and pressure were determined with accuracies of ± 0.3 GPa and ± 7 °C, respectively, in the quasihydrostatic case and with ± 0.02 GPa and ± 1.5 °C in the hydrostatic case. Before the high-pressure experiments, each $Zn_{41}Sb_{59}$ sample was investigated by x-rays at room temperature to ensure that no crystalline phases were present.

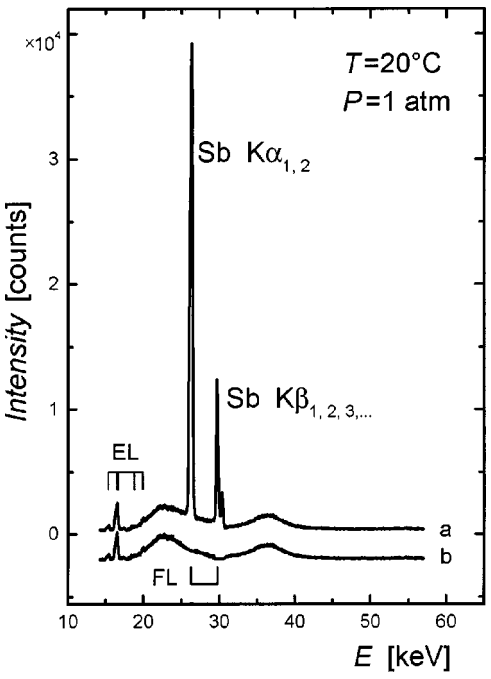

FIG. 1. (a) Experimental EDXD spectrum of amorphous $Zn_{41}Sb_{59}$ in the diamond-anvil cell at ambient conditions. (b) The same spectrum after subtraction of the fluorescence lines. This spectrum is given here for comparison and is shown on a larger scale in Fig. 2 by the curve labelled ''0 GPa.'' The diffraction angle is $2\Theta = 9.7174°$. Positions of the fluorescence lines (FL) and of the escape lines (EL) are indicated with vertical bars.

III. EXPERIMENTAL RESULTS

A. High-pressure x-ray studies

Curve *a* in Fig. 1 shows the EDXD spectrum of the initial amorphous $Zn_{41}Sb_{59}$ sample in the DAC before application of pressure. In addition to the diffraction pattern from $Zn_{41}Sb_{59}$, the spectrum contains two groups of strong fluorescence lines (FL) of Sb at 26.3 and 29.8 keV and a number of escape lines (EL) generated in the Ge detector. The diffraction angle $2\Theta = 9.7174°$ was chosen for minimum overlap of the fluorescence lines with the diffraction halos of amorphous $Zn_{41}Sb_{59}$.

The profile of the pressure-independent fluorescence lines was derived from the EDXD spectra of crystalline γ-$Zn_{41}Sb_{59}$measured in a separate experiment, using a larger angle of $2\Theta = 11.566°$ to avoid overlap of fluorescence and diffraction lines. This profile is subtracted from all the measured spectra for a more accurate evaluation of the shape and position of the diffraction halos of amorphous $Zn_{41}Sb_{59}$. Curve *b* in Fig. 1 shows the resulting spectrum for ambient conditions and the whole set of the resulting spectra is presented in Fig. 2.

The weak escape lines, which are also pressure independent, are not removed from the spectra in Fig. 2 and can serve as reference marks. The spectrum measured at 6.3 GPa contains one more detectable escape line positioned at ≈ 18 keV, which results from the (001) line of the γ phase. Additionally, most spectra exhibit weak and yet unidentified lines near 22.2 and 34.7 keV, which do not move with pressure and therefore do not belong to the diffraction pattern of the $Zn_{41}Sb_{59}$ sample.

As seen from Fig. 2, at room temperature and pressures up to 5.4 GPa, the spectra of $Zn_{41}Sb_{59}$ consist of two halos characteristic of amorphous materials. At a pressure of 6.0 GPa, the sample partly crystallized to a mixture of ZnSb +Sb, and a peak composed of the strongest (112) and (121) lines of ZnSb and of the strongest (102) line of Sb appeared in the region of the first halo. At 6.3 GPa, the intensity of this peak was approximately the same whereas the amorphous phase mostly transformed to the simple hexagonal γ phase with the lattice parameters $a = 3.028(5)$ Å and $c = 2.760(5)$ Å in good agreement with previous results.[6]

The structure factor $S(Q)$, where Q is the momentum transfer, for amorphous $Zn_{41}Sb_{59}$ prepared by the same method as in this work was accurately determined earlier at ambient pressure by neutron diffraction.[14] Figure 3 depicts these data together with the structure factor for the initial ambient pressure $Zn_{41}Sb_{59}$ sample calculated from the present EDXD data without corrections for the energy dependence of the incident beam intensity. It is seen that the positions and the widths of the first two halos are very similar in both $S(Q)$ spectra. This comparison leads to the conclusion that the position and the width of these halos for $Zn_{41}Sb_{59}$ under pressure also can be determined reasonably well from the EDXD spectra.

As is seen from Fig. 2, the width of both diffraction halos does not change significantly with pressures up to 6 GPa. The half-width ΔQ_1 of the first halo of $S(Q)$ can be used to give an estimate for the correlation length Δx_i of the atomic short-range order in $Zn_{41}Sb_{59}$ according to the Scherrer formula $\Delta x_i = 2\pi/\Delta Q_1$. The resulting value of Δx_i

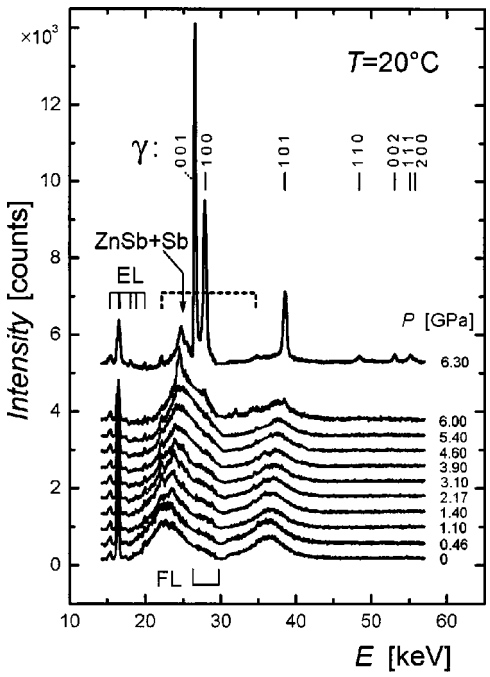

FIG. 2. The EDXD spectra of the initially amorphous $Zn_{41}Sb_{59}$ alloy measured at room temperature and different pressures in the course of a stepwise pressure increase in a diamond-anvil cell using a diffraction angle of $2\Theta = 9.7174°$. The fluorescence lines occurring in all spectra at around 26.3 and 29.8 keV have been subtracted, their positions (FL) and the positions of the escape lines (EL) are indicated with solid vertical bars. The dotted bars indicate the positions, ≈ 22.2 keV and ~ 34.7 keV, of two weak unidentified lines present in most spectra. The letter γ labels the Miller indices of the hexagonal γ phase formed at 6.3 GPa.

$\sim 11-12$ Å remains constant for $Zn_{41}Sb_{59}$ within the pressure interval 0–6 GPa and is typical for amorphous materials.

Figure 4 shows the pressure dependences of the positions of both diffraction halos of amorphous $Zn_{41}Sb_{59}$ in units of interatomic distances $d = 2\pi/Q$. Both dependences are approximately linear at $P < 1.5$ GPa and at $P > 1.5$ GPa. The breaks in the slopes of both dependences are observed at about the same pressure of 1.45 GPa which is indicative of some qualitative change in the amorphous state of the sample occurring at room temperature in the vicinity of this pressure. Further investigations (Sec. III B) showed that this is the same $am_1 \rightarrow am_2$ transition observed previously,[4] but shifted to a lower pressure due to the more hydrostatic conditions of the present experiments. Note that the larger slopes $|\partial d/\partial P|$ of both $d(P)$ dependences for the am_1 phase correlate with its larger compressibility of about 0.026 GPa^{-1} compared to about 0.016 GPa^{-1} for the am_2 phase.[4]

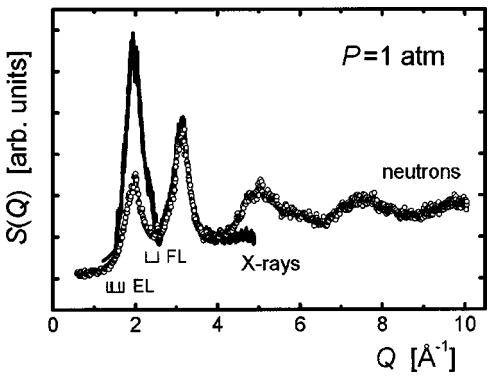

FIG. 3. The structure factor $S(Q)$ for amorphous $Zn_{41}Sb_{59}$ at ambient pressure. The open circles represent the result (Ref. 14) of the neutron-diffraction measurement at 100 K. The solid line illustrates the x-ray data of this work shown in Fig. 2 by the curve ''0 GPa,'' both fluorescence and escape lines are removed.

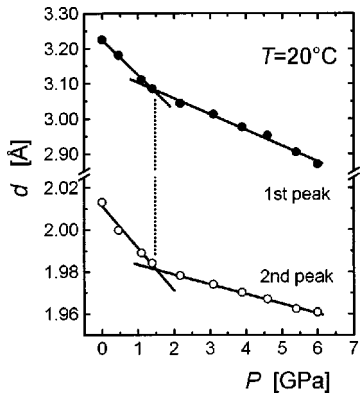

FIG. 4. The effect of pressure on the positions $d = 2\pi/Q$ of the centres of gravity for the first and second diffraction peaks in the EDXD spectra of amorphous $Zn_{41}Sb_{59}$ shown in Fig. 2. The diameter of the circles around data points corresponds to the experimental error.

Nearly invariable width of amorphous halos in the diffraction patterns of $Zn_{41}Sb_{59}$ throughout the studied pressure interval suggests that the am_2 state is single phase and that the am_2 phase therefore has the same composition as the am_1 phase. In fact, if the am_2 state were a mixture of amorphous phases with different compositions and, correspondingly, different diffraction patterns, one could expect at least a noticeable broadening of the amorphous halos after the $am_1 \rightarrow am_2$ transition.

B. *T-P* diagram of amorphous $Zn_{41}Sb_{59}$

Figure 5 presents the *T-P* diagram for the phase transitions in the initially amorphous $Zn_{41}Sb_{59}$. The diagram combines the data of electrical resistance measurements with the results of high-pressure EDXD experiments and the x-ray examination of quenched samples at ambient pressure and 100 K.

The temperatures of crystallization of amorphous $Zn_{41}Sb_{59}$ at different pressures (asterisks in Fig. 5) correspond to the midpoints of the step in the isobars of electrical resistance measured at increasing temperature. Three representative isobars are shown in Fig. 6. In the course of the measurement, the sample was held at each point until the slope of the $\log_{10}\rho$ versus time decreased by a factor of 10, and the final value of $\log_{10}\rho$ was plotted in the figure. This process took 1–5 h within the interval of crystallization, 10–20 min below and above this interval, and less than 5 min on further cooling of the crystallized sample.

According to the DSC and dilatometric data,[4] crystallization of amorphous $Zn_{41}Sb_{59}$ to a mixture of ZnSb + Sb on heating at a rate of 5 °C/min at ambient pressure occurred in the temperature interval 180–230 °C. As is seen in Fig. 5, in

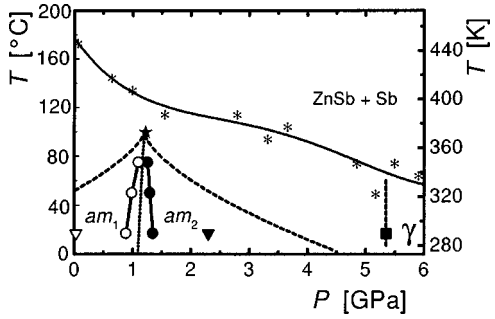

FIG. 5. *T-P* phase diagram for initially amorphous $Zn_{41}Sb_{59}$. am_1 and am_2 are the low- and high-pressure amorphous semiconductor phases, γ is the high-pressure semimetal phase with a simple hexagonal lattice. The solid square stands for the $am \rightarrow \gamma$ transition at increasing pressure. The asterisks show the positions of the irreversible transitions of am and γ phases to a mixture of ZnSb + Sb at increasing temperature. The solid and open circles indicate the $am_1 \rightarrow am_2$ and $am_2 \rightarrow am_1$ transitions at increasing and decreasing pressure under hydrostatic conditions, the solid and open triangles show where these transitions occur under quasihydrostatic conditions.[4] The star marks the tentative position of the critical point of the $am_1 \rightleftarrows am_2$ line. The two dashed lines starting from this point are the calculated spinodals.

the present experiments with much lower heating rate, this process is already mostly completed at 180 °C. An increase in pressure leads to a significant decrease in the crystallization temperature down to about 80 °C at 5 GPa.

An increase in pressure in excess of 5 GPa at room temperature results in crystallization of amorphous $Zn_{41}Sb_{59}$ into the γ phase. The solid square in Fig. 5 represents the midpoint of the isothermal change for the electric resistance measured in the course of a stepwise increase in pressure with exposure times for every point depending on the $\log_{10}\rho$ drift which continued for 1–3 h in the vicinity of the step and for 15–20 min otherwise. The shape of the $\log_{10}\rho(P)$ dependence and the position of the step were close to those observed earlier.[4] However, the step occurred in both cases at a pressure of about 5.4 GPa which is much lower than the pressure of about 6.3 GPa for the formation of the γ phase in the EDXD experiment, Fig. 2. Besides, at about 6 GPa the amorphous phase in the EDXD experiment was partly transformed to a mixture of ZnSb + Sb. This mixture was never formed at room temperature in the electric resistance

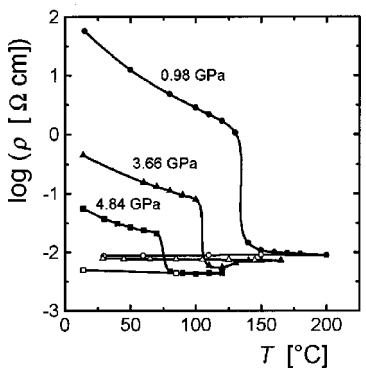

FIG. 6. The isobars of the electric resistivity, ρ, measured on stepwise heating (solid symbols) and cooling (open symbols) of the initially amorphous $Zn_{41}Sb_{59}$ samples.

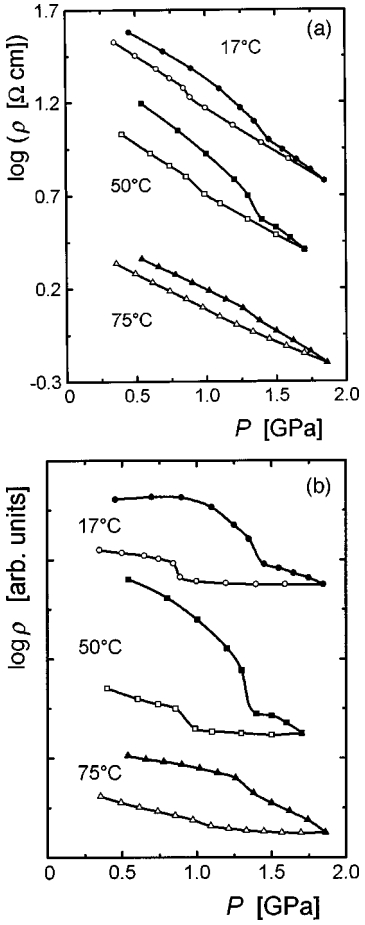

FIG. 7. (a) The isotherms of the electric resistivity, ρ, of the amorphous $Zn_{41}Sb_{59}$ sample measured under hydrostatic conditions in the course of a stepwise increase (solid symbols) and decrease (open symbols) in pressure. (b) The same isotherms modified to gain better visualization of the regions of phase transitions: the slope of each isotherm is reduced by subtracting a linear function adjusted to the initial portion of the curve measured at decreasing pressure.

measurements[4] because the sample crystallized to the γ phase at a lower pressure. The lower formation pressure of the γ phase in the course of the electric resistance measurements resulted presumably from quasihydrostatic conditions of these experiments in contrast to nearly hydrostatic conditions of the EDXD experiments.

The pressures for the transitions between the amorphous phases (circles in Fig. 5) represent the positions of the steepest portions of the electrical resistance isotherms (Fig. 7) measured under hydrostatic conditions. In comparison with the measurements under quasihydrostatic conditions[4] (triangles in Fig. 5), one may notice a better accuracy of the transition pressure and temperature and, what is most important, an essential decrease in the hysteresis of the $am_1 \rightleftarrows am_2$ transformation thus providing a better localization of the $am_1 \rightleftarrows am_2$ equilibrium line given in Fig. 5 by the short-dashed line.

The electrical resistance isotherms shown in Fig. 7 were measured with increasing and decreasing pressure in steps of 0.1 GPa. At 17 and 50 °C, the sample was kept at each point until a tenfold decrease in the slope of the $\log_{10}\rho$ versus time was obtained, which took from 1 h at the edges of the studied

pressure interval to 15 h near the steepest portions of the $\log_{10}\rho(P)$ dependences. At 75 °C, partial crystallization of the sample to a mixture of ZnSb + Sb contributed noticeably to the time dependence of $\log_{10}\rho$, and the 75 °C isotherm was measured in an isochronic regime, by holding the sample at each given pressure for 3 h. Figure 7 shows the final $\ln\rho$ values.

IV. DISCUSSION

From a structural point of view, the only difference between amorphous phases with the same composition, like those in $Zn_{41}Sb_{59}$, is their different short-range order. Therefore equilibria between such amorphous phases should be of the same type as those between different phases in one-component liquids which are considered as ''liquid-liquid'' or ''vapor-liquid'' equilibria depending on the density of the constituent phases. On the *T*-*P* diagrams, the lines of these equilibria terminate either in a point of intersection with another equilibrium line or in a critical point. The behavior of the electrical resistance of amorphous $Zn_{41}Sb_{59}$ suggests that the line of the $am_1 \rightleftarrows am_2$ equilibrium terminates in a critical point and that the critical temperature is of the order of 100 °C as indicated by the star in Fig. 5.

In fact, the $am_1 \rightarrow am_2$ and $am_2 \rightarrow am_1$ transitions are very sluggish and no acceleration is observed with increase in temperature from 17 to 75 °C. At the same time, the rate of crystallization to a mixture of ZnSb + Sb becomes noticeable at 75 °C though this process requires diffusion of atoms over much longer distances than in the course of the isoconcentrational $am_1 \rightleftarrows am_2$ transformation. A significant decrease in the mobility of atoms is characteristic of systems approaching critical points. Therefore the critical temperature of the $am_1 \rightleftarrows am_2$ transformation should not be far above 75 °C.

With kinetics of isomorphic phase transitions as sluggish as in the case of amorphous $Zn_{41}Sb_{59}$, one can expect that the $am_1 \rightleftarrows am_2$ transformation exhibits a clearly visible hysteresis until the volume effect of this transformation is zero, i.e., until the critical temperature is reached. As is seen from Fig. 5, linear extrapolations of the lines of the $am_1 \rightarrow am_2$ and $am_2 \rightarrow am_1$ transitions give zero hysteresis at a temperature of about 100 °C.

A fortunate feature of isomorphic transformations is the fact that the thermodynamic properties of both phases can be well described in many cases with one and a rather simple model Gibbs potential. In particular, these models allow a determination of spinodals which are useful for a better understanding of the hysteresis phenomena. Specifically, a simple two-level model which was first developed to describe the *T*-*P* diagram of cerium undergoing an isomorphic phase transition[15] and then was successfully applied to the transition between amorphous phases of ice,[8] will be applied here to the present case.

The basic concept of this model assumes that both amorphous phases consist of clusters of two types, corresponding to the (hypothetical) short-range order in the first and in the second phase, respectively, at $T=0$ K. These clusters are considered as two components of the amorphous system and the Gibbs potential, $G(x)$, is written in the approximation of regular solutions. However, by contrast to the standard approximation of regular solutions, the concentration x is not an independent variable, but its value is determined by the minimum conditions: $\partial G/\partial x = 0$ and $\partial^2 G/\partial x^2 > 0$.

As a function of x, the Gibbs potential can have one or two minima depending on the *T*-*P* region. Two minimum values of $G(x)$ are equal along a straight line which represents the first-order phase transformation between the two amorphous phases and terminates in a critical point at T_{cr} where the two minima coincide and $x_1 = x_2 = 1/2$. The points on the *T*-*P* plane, where one of the two minima of $G(x)$ degenerates to an inflection point, form two lines starting from the critical point. These are spinodals, or the lines of complete loss of thermodynamic stability of one of the phases.

The Gibbs potential thus constructed can be specified in a unique fashion by the values of four parameters:[8,15] U, ΔV, ΔS, and ΔE_0, where $U = 2RT_{cr}$ is the mixing energy, ΔV and ΔS are the volume and entropy effects of the transition at any given temperature, ΔE_0 is the difference between the internal energies of the components at 0 K. If, as discussed above, one adopts $T_{cr} = 373$ K and, correspondingly, $U = 6.2$ kJ/mol, the other three constants can be derived from experiment.

The volume effect of $\Delta V/V \approx 0.8\%$ of the $am_1 \rightarrow am_2$ transition at room temperature has been measured before.[4] The specific volume of $V = 16.4(1)$ cm^3/mol of the am_1 phase at ambient conditions was determined by hydrostatic weighing in this work. Therefore $\Delta V = 0.13$ cm^3/mol. With the line of the $am_1 \rightleftarrows am_2$ equilibrium drawn in the middle between the hysteresis branches (Fig. 5), a value of $\Delta S = -0.14$ J/(K mol) can be obtained from the Clapeyron equation $dT/dP = \Delta V/\Delta S$. The difference between the internal energies of the components at 0 K can be estimated as $\Delta E_0 = -P_0 \Delta V_0 = 0.14$ kJ/mol, where $P_0 = 0.8$ GPa results from a linear extrapolation of the $am_1 \rightleftarrows am_2$ line to 0 K. $\Delta V_0 = 0.17$ cm^3/mol is the volume discontinuity at the $am_1 \rightarrow am_2$ transition at 0 K calculated from the room-temperature value of $\Delta V = 0.13$ cm^3/mol by using the temperature dependence of the ratio of $\Delta V(T)/\Delta V(0)$ which is a unique function of the T/T_{cr} ratio in the model used.

The spinodals calculated with these values of the model parameters are plotted as dashed lines in Fig. 5. The am_1 state is no longer a phase above the spinodal on the right side of the critical point and the am_2 state cannot exist above the left spinodal. Actually, the spinodals outline the temperature dependence of the maximum possible hysteresis of the transformation.

As is seen from Fig. 5, the hysteresis observed in the experiments is much smaller than the distance between the spinodals. At the same time, the large span of the spinodals shows that the thermodynamic stability of the am_1 and am_2 phases changes slowly over this large pressure interval, so the hysteresis of the $am_1 \rightleftarrows am_2$ transformation can be effectively influenced by other factors. This is illustrated in Fig. 5 by the fourfold decrease in the room-temperature hysteresis under hydrostatic conditions compared to the one observed in the presence of shear stresses in experiments with quasi-hydrostatic high pressures.[4]

The Gibbs potential, once constructed, allows a calculation of all thermodynamic properties of the system and, in particular, of the anomalies in the temperature dependences

of the volume and of heat capacity at ambient pressure related to the $am_1 \rightleftarrows am_2$ transformation. However, in amorphous $Zn_{41}Sb_{59}$ these anomalies cannot be observed because the am_1 phase transforms on heating above 50 °C into one more amorphous modification, other than am_2, and this transformation is accompanied by a volume increase of a few percent and by a rather large heat release.[4] The transformation is irreversible at atmospheric pressure, but at high pressures and room temperature the am_1 phase is formed again long before the $am_1 \rightarrow am_2$ transition occurs.[4]

With respect to the occurrence of three different amorphous semiconductor phases in the $Zn_{41}Sb_{59}$ alloy, one should note the following: In the Zn-Sb system, there are three semiconductor compounds, ZnSb, Zn_4Sb_3 and Zn_3Sb_2, and the latter two have even various polymorphic modifications.[9] Therefore the characteristic feature of this system is, that many different crystal structures have close values of the Gibbs free energy. On the other hand, there is an empirical rule for glasses, saying that the local atomic structure of a glass is similar to that of one of the crystalline forms of the material.[16] The am_1 phase has the same type of local atomic structure as crystalline ZnSb compound.[14] One could expect that the two other amorphous phases also are analogs of certain crystalline phases in the Zn-Sb system and that these amorphous phases have values of the Gibbs free energy close to the one of the am_1 phase. If this is the case, the relative stability of amorphous phases in $Zn_{41}Sb_{59}$ should strongly depend on temperature and pressure, and phase transitions between different amorphous phases can occur even within the rather limited *T-P* region of their thermal stability.

V. SUMMARY

The *T-P* region of thermal stability of amorphous $Zn_{41}Sb_{59}$ is shown to be bounded on the high-temperature side by a line of crystallization resulting in a mixture of ZnSb + Sb. This line descends from about 180 °C at ambient pressure to about 80 °C at 5 GPa. At pressures exceeding 5–6 GPa, amorphous $Zn_{41}Sb_{59}$ crystallizes to the γ phase with a simple hexagonal structure. Inside the region bounded by the crystallization lines, a reversible first-order phase transition between two different amorphous phases, am_1 and am_2, with the same $Zn_{41}Sb_{59}$ composition is found to occur at pressures around 1 GPa. The line of the $am_1 \rightleftarrows am_2$ metastable equilibrium is experimentally determined at temperatures from 17 to 75 °C and evidences are given that this line terminates in a critical point at a temperature of about 100 °C. Within the framework of a two-level model, the Gibbs potential of amorphous $Zn_{41}Sb_{59}$ is constructed and the lines of a complete loss of thermodynamic stability (spinodals) are calculated for both amorphous phases. The given *T-P* diagram is the first example of a diagram with a line of phase equilibrium between two different amorphous semiconductor phases.

ACKNOWLEDGMENTS

This work was supported by Grant Nos. 99-02-17007 and 96-15-96806 from the Russian Foundation for Basic Research and by Grant No. 34-1997 for young scientists from the Russian Academy of Sciences. One of the authors (O.I.B.) thanks the Alexander von Humboldt Foundation for support and thanks HASYLAB for financial support and the hospitality during his stay at DESY, Hamburg. Financial support by the German Ministry of Research and Technology under Contract No. 05647PPA is gratefully acknowledged. The authors are grateful to Professor W. B. Holzapfel and G. Grosse for helpful discussions and would like to thank W. Bröckling for technical assistance.

*Present address: Fachbereich Physik, Universität-GH-Paderborn, D-33095 Paderborn, Germany.

[1] I.T. Belash and E.G. Ponyatovsky, High Temp.-High Press. **9**, 651 (1977).

[2] E.G. Ponyatovsky, I.T. Belash, and O.I. Barkalov, J. Non-Cryst. Solids **117&118**, 679 (1990).

[3] E.G. Ponyatovsky and O.I. Barkalov, Mater. Sci. Rep. **8**, 147 (1992).

[4] V.E. Antonov, A.E. Arakelyan, O.I. Barkalov, A.F. Gurov, E.G. Ponyatovsky, V.I. Rashupkin, and V.M. Teplinsky, J. Alloys Compd. **194**, 279 (1993).

[5] V.E. Antonov, O.I. Barkalov, E.G. Ponyatovsky, and S.A. Zavolovich, High Press. Res. **15**, 201 (1997).

[6] V.F. Degtyareva, I.K. Bdikin, and S.S. Khasanov, Fiz. Tverd. Tela **39**, 1509 (1997) [Sov. Phys. Solid State **39**, 1341 (1997)].

[7] O. Mishima, L.D. Calvert, and E. Whalley, Nature (London) **310**, 393 (1984).

[8] E.G. Ponyatovskii, V.V. Sinitsyn, and T.A. Pozdnyakova, Pis'ma Zh. Éksp. Teor. Phys. **60**, 352 (1994) [JETP Lett. **60**, 360 (1994)].

[9] M. Hansen and K. Anderko, *Constitution of Binary Alloys* (McGraw-Hill, New York, 1958).

[10] I.T. Belash, V.F. Degtyareva, E.G. Ponyatovskii, and V.I. Rashupkin, Fiz. Tverd. Tela **29**, 1788 (1987) [Sov. Phys. Solid State **29**, 1028 (1987)].

[11] K. Syassen and W.B. Holzapfel, Europhys. Conf. Abstr. **1A**, 75 (1975).

[12] W. B. Holzapfel, in *High Pressure Chemistry*, edited by H. Kelm (Reidel, Boston, 1978), p. 177.

[13] H.K. Mao, P.M. Bell, J.W. Shaner, and D.J. Steinberg, J. Appl. Phys. **49**, 3276 (1978).

[14] O.I. Barkalov, A.I. Kolesnikov, E.G. Ponyatovsky, U. Dahlborg, R. Delaplane, and A. Wannberg, J. Non-Cryst. Solids **176**, 263 (1994).

[15] I.L. Aptekar and E.G. Ponyatovsky, Dokl. Akad. Nauk SSSR **173**, 851 (1967) (in Russian).

[16] C.N.J. Wagner, J. Non-Cryst. Solids **42**, 3 (1980).